Impact of the Vertical Variation of Cloud Droplet Size on the Estimation of Cloud Liquid Water Path and Rain Detection

RUIYUE CHEN

Department of Atmospheric and Oceanic Sciences, Cooperative Institute for Climate Studies, University of Maryland, College Park, College Park, Maryland

FU-LUNG CHANG

National Institute for Aerospace, Hampton, Virginia

ZHANQING LI

Department of Atmospheric and Oceanic Sciences, Cooperative Institute for Climate Studies, University of Maryland, College Park, College Park, Maryland

RALPH FERRARO

Cooperative Institute for Climate Studies, University of Maryland, College Park, and NOAA/NESDIS/Center for Satellite Applications and Research, Camp Springs, Maryland

FUZHONG WENG

NOAA/NESDIS/Center for Satellite Applications and Research, Camp Springs, Maryland

(Manuscript received 18 April 2006, in final form 26 January 2007)

ABSTRACT

Cloud droplet effective radius (DER) and liquid water path (LWP) are two key parameters for the quantitative assessment of cloud effects on the exchange of energy and water. Chang and Li presented an algorithm using multichannel measurements made at 3.7, 2.1, and 1.6 μm to retrieve a cloud DER vertical profile for improved cloud LWP estimation. This study applies the multichannel algorithm to the NASA Moderate Resolution Imaging Spectroradiometer (MODIS) data on the *Aqua* satellite, which also carries the Advanced Microwave Scanning Radiometer (AMSR-E) for measuring cloud LWP and precipitation. By analyzing one day of coincident MODIS and AMSR-E observations over the tropical oceans between 40°S and 40°N for overcast warm clouds (>273 K) having optical depths between 3.6 and 23, the effects of DER vertical variation on the MODIS-derived LWP are reported. It is shown that the LWP tends to be overestimated if the DER increases with height within the cloud and underestimated if the DER decreases with height within the cloud. Despite the uncertainties in both MODIS and AMSR-E retrievals, the result shows that accounting for the DER vertical variation reduces the mean biases and root-mean-square errors between the MODIS- and AMSR-E–derived LWPs. Besides, the manner in which the DER changes with height has the potential for differentiating precipitative and nonprecipitative warm clouds. For precipitating clouds, the DER at the cloud top is substantially smaller than the DER at the cloud base. For nonprecipitating clouds, however, the DER differences between the cloud top and the cloud base are much less.

1. Introduction

It has long been recognized that clouds play a dominant role in the earth's climate and its changes. Clouds strongly affect the energy balance and water cycle, two dominant processes in the climate system. Low-level boundary layer clouds have the most significant influence on cloud radiative forcing because of their areal extent and frequency (Harrison et al. 1990; Hartmann et al. 1992). Radiation absorbed by boundary layer clouds also plays an important role in the evolution of cloud systems and affects water redistribution (Stephens 1999). The effect of boundary layer clouds is

---

Corresponding author address: Zhanqing Li, Department of Atmospheric and Oceanic Sciences, University of Maryland, College Park, College Park, MD 20742.
E-mail: zli@atmos.umd.edu

so strong that even small changes in their optical and microphysical properties are likely to have major consequences for climate change. The liquid water path (LWP) is an important cloud microphysical property that determines the climatic effects of boundary layer clouds. For example, Greenwald et al. (1995) found that a 0.05 kg m^{-2} increase in LWP (for LWP < 0.2 kg m^{-2}) results in a -25 W m^{-2} change in the net cloud forcing at a solar zenith angle of 75°. Satellites provide the only means of acquiring global and long-term LWP estimates. The LWP is estimated from satellite measurements of either microwave radiation emitted by the cloud or visible/near infrared (NIR) solar reflectance from the cloud.

Beginning in the 1980s, several efforts have been made to determine the global distribution of cloud LWP from satellite microwave measurements, such as those made by the Special Sensor Microwave Imager (SSM/I) on the Defense Meteorological Satellites (Wentz 1997), the Advanced Microwave Sounding Unit (AMSU) on the National Oceanic and Atmospheric Administration (NOAA) *NOAA-15*, *-16*, and *-17* platforms (Grody et al. 2001; Ferraro et al. 2005), and the Advanced Microwave Scanning Radiometer (AMSR-E; Ashcroft and Wentz 2000) on the *Aqua* satellite. These algorithms utilize the microwave signature emitted by cloud droplets. Microwave retrievals of cloud LWP are not applicable over land because of the strong and highly variable microwave emission of the land surface. The emission from ocean surfaces is less variable, so cloud LWP can be estimated from satellite-observed microwave radiances. However, LWP retrieval accuracy is affected by the sea surface temperature, surface wind speed, atmospheric precipitable water vapor, and radiometric calibration while uncertainties in the absorption coefficients used in the microwave radiative transfer model also affect the accuracy of LWP estimation from microwave observations (Lin and Rossow 1994; Marchand et al. 2003). Since microwave LWP estimation is based on the radiances emitted by cloud water droplets, it is applicable for observations during the day and night.

Cloud LWP can also be estimated from solar reflectance measurements made during the daytime. In the visible/NIR method (Nakajima and King 1990; Han et al. 1998), cloud LWP is derived based on the products of cloud optical depth and droplet effective radius (DER). The retrieval of cloud optical depth utilizes the reflectance measurement at a visible channel and the retrieval of DER utilizes the reflectance measurements at a NIR channel. Some earlier studies estimated cloud LWP using the cloud optical depth retrieval but assuming a constant DER equal to 10 μm because of a lack of

reliable DER retrievals (e.g., Rossow 1989; Lin and Rossow 1994). After the launch of the Advanced Very High Resolution Radiometer (AVHRR), the 3.7-μm channel has been widely used to retrieve DER information (Kaufman and Nakajima 1993; Han et al. 1994; Platnick and Valero 1995). However, the 3.7-μm measurements are most sensitive to droplet absorption occurring near the cloud top, their DER retrievals mainly represent the cloud-top portion, which may not represent the entire DER profile for the whole cloud column. Since LWP is defined as a column-integrated quantity, use of the 3.7 μm DER retrieval can cause biases in the LWP estimation when the DER varies vertically within a cloud.

Relative to the AVHRR, the Moderate Resolution Imaging Spectroradiometer (MODIS) onboard the *Terra* and *Aqua* platforms has numerous advances that considerably improve the retrievals of cloud properties. They include, among many others, onboard calibration and 36-channel high spectral and spatial resolutions. Three channels are used for cloud DER retrievals, namely, 1.6, 2.1, and 3.7 μm. Because of the varying strengths of cloud absorption at these different spectral channels, the three channels have different reflectance weighting functions from cloud top to cloud base (Platnick 2000). The weighting function for 3.7 μm is mainly confined to the cloud-top layer, while the weighting function for 1.6 μm spreads more evenly into the lower cloud layer. Consequently, the 3.7-μm retrieval corresponds to the DER at the very top of the cloud layer, whereas the 2.1- and 1.6-μm retrievals are determined by DER values from the cloud top to deeper layers inside the cloud.

Assuming that the DER has a linear variation in the vertical direction, Chang and Li (2002) presented a method to determine an optimal linear DER profile by using a combination of multiple NIR-channel measurements. Their simulations with in situ observed DER profiles and sensitivity studies showed that the method is most effective for clouds with near-linear DER profiles, which are shown by the majority of in situ measurements (Miles et al. 2000). When the clouds are very thick and the cloud DER profiles are very nonlinear, the estimation of DER at the cloud base would involve large uncertainties because the signal from the cloud base is weak and the assumption of a linear DER profile is invalid. In a later paper on case studies, Chang and Li (2003) also examined some modified assumptions for the linear DER profile, and they found that the retrieval of DER profile shows improvements over the LWP calculations by taking advantage of the three NIR channels instead of one for which a constant DER must be assumed.

This study applies the modified algorithm of Chang and Li (2003) to the MODIS observations over oceans and examines the MODIS LWP estimation. The impact of cloud DER vertical variation on the MODIS LWP is evaluated through comparisons between MODIS-derived and AMSR-E–derived LWPs. The potential impact of the DER profile on warm rain detection is also discussed.

This investigation is a prelaunch study for the Geostationary Operational Environmental Satellite-R (GOES-R), which is currently scheduled for launch in 2012. The Advanced Baseline Imager (ABI) on GOES-R has similar channels to MODIS (e.g., 0.64, 1.61, 2.26, and 3.90 μm). The DER profile retrieval algorithm is applicable to those channels and enhances the accuracy of retrievals from GOES-R, such as rain detection and LWP estimations.

2. Data and methodology

Data collected on 1 January 2003 from MODIS and AMSR-E instruments on *Aqua* (which was launched on 4 May 2002) are used in this investigation. The investigation is limited to warm clouds over tropical oceans (40°N–40°S). To eliminate ice contamination, only warm liquid water clouds (cloud-top temperatures > 273 K) are selected. To minimize the impact of cloud three-dimensional (3D) effects, we utilize MODIS measurements with satellite viewing angles less than 30° and solar zenith angles less than 50°.

a. MODIS retrieval

Traditionally, cloud LWP is derived using retrievals of cloud optical depth, τ, and droplet effective radius, r_e, as given by

$$\text{LWP} = \frac{4\rho_w}{3Q_e}\tau r_e, \qquad (1)$$

where τ and r_e are defined by (Hansen and Travis 1974)

$$\tau = \int\int Q_e n(r)\pi r^2 \, dr \, dz \qquad (2)$$

$$r_e = \frac{\int \pi r^3 n(r) \, dr}{\int \pi r^2 n(r) \, dr}. \qquad (3)$$

Here, ρ_w is the density of liquid water, Q_e is the extinction efficiency and is equal to the constant 2, z is the altitude, r is the droplet radius, and $n(r)$ is the droplet number distribution between r and dr. The LWP calculated by Eq. (1) assumes that r_e is vertically constant.

In this study, MODIS 1-km L1B data (version 4) are utilized to retrieve cloud properties. The cloud optical depth, τ, is retrieved from the MODIS 0.86-μm reflectance measurement for the clouds over ocean. The selection of the 0.86-μm channel reduces uncertainties of the cloud optical depth retrieval because ocean surface reflectances are small and less variable at the 0.86-μm channel (King et al. 2003). Three different cloud DER values, namely, $r_{e3.7}$, $r_{e2.1}$, and $r_{e1.6}$, are retrieved using a single NIR channel from each of the MODIS measurements at 3.7, 2.1, and 1.6 μm. Following the method of Chang and Li (2003), a linear DER vertical profile (DVP) defined by a cloud-top DER and a cloud-bottom DER is also retrieved using a combination of all three NIR channels. The cloud-top temperature is retrieved from the 11-μm brightness temperature measurement. Atmospheric effects are corrected using the temperature and humidity profiles obtained from the MODIS 07 (MOD07, version 4) atmospheric products (Menzel and Gumley 1998), which are mainly obtained from the National Centers for Environmental Prediction (NCEP) Global Data Assimilation System (Derber et al. 1991). The effects of thin cirrus contamination are eliminated using the cirrus detection reported in the MOD06 cirrus product (King et al. 2003).

The single NIR retrieval of $r_{e3.7}$ follows the iterative method of Chang et al. (2000) applied earlier to the AVHRR data, which is similar to the methods of Han et al. (1994) and Platnick and Valero (1995). In the method, the retrievals of cloud optical depth, DER, and top temperature are applied through an iterative procedure to determine the optimal retrievals. The retrievals of $r_{e2.1}$ and $r_{e1.6}$ in this study essentially follow the same method as the retrieval of $r_{e3.7}$, except that the 3.7-μm measurement contains both emission and reflection. The contribution of the 3.7-μm emission is calculated using radiative transfer modeling with cloud-top temperature retrieved from the 11-μm channel. Platnick and Valero (1995) provided a detailed discussion on the uncertainties of the retrieved cloud optical depth and DER. They showed that the accuracy of the optical depth retrieval is primarily affected by the visible-channel reflectance uncertainties and the accuracy of the DER retrieval is primarily affected by the NIR-channel reflectance uncertainties. A visible reflectance error of 5% causes a 10% error for typical cloud optical depths ~5–20, but large changes in cloud optical depth can occur for small changes in the reflectance for thick clouds. An NIR reflectance error of 5% causes a similar magnitude of error in DER. However, large errors in both DER and optical depth can occur for thin clouds. The calibration errors for MODIS data are expected to be less than 2% (King et al. 1997). Some modeling
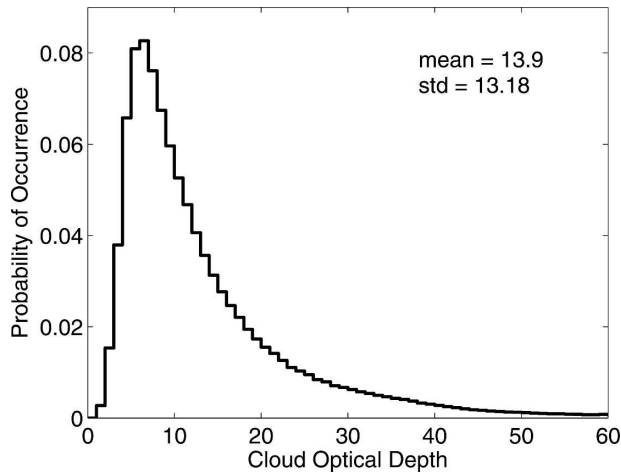
FIG. 1. Probability density function of cloud optical depth.

FIG. 2. Probability density function of DER retrieved from one of the NIR channels.

errors may also result in uncertainties that are estimated to be on the order of 10% for the retrieval of DER and on the order of 15% for the retrieval of cloud optical depth (King et al. 1997; Rossow et al. 1989).

Figure 1 shows the frequency distribution of the overcast cloud optical depth retrieved from the 1-km MODIS 0.86-μm reflectance and Fig. 2 compares the frequency distributions of the three DERs ($r_{e3.7}$, $r_{e2.1}$, and $r_{e1.6}$) retrieved from each of the MODIS 3.7-, 2.1-, and 1.6-μm channels. The overcast clouds are defined over an AMSR-E footprint ($\sim$13 km $\times$ 7 km) and only successful DER retrievals from all three NIR channels are included in Figs. 1 and 2. The mean cloud optical depth is 13.9 ($\pm$13.2) with a maximum occurrence at $\sim$8. The mean DER increases from $r_{e3.7} = 13.0$ μm to $r_{e2.1} = 13.4$ μm and to $r_{e1.6} = 13.8$ μm. The spread (standard deviations, hereafter referred to as "std" in the figures and tables) of the distribution also increases from $r_{e3.7}$ to $r_{e2.1}$ and to $r_{e1.6}$. The RMS differences in the DER are 1.1 μm between $r_{e3.7}$ and $r_{e2.1}$, 1.2 μm between $r_{e2.1}$ and $r_{e1.6}$, and 2.2 μm between $r_{e3.7}$ and $r_{e1.6}$.

To account for the vertical variation of r_e following the method of Chang and Li (2003), a linear r_e profile is retrieved using combined information from the multi-NIR channels at 3.7, 2.1, and 1.6 μm. Here, the linear r_e profile is defined as a function of height, z, by

$$r_e(z') = r_{e1} + (r_{e2} - r_{e1})z', \qquad (4)$$

where $z' = (z - z_{\text{top}})/(z_{\text{base}} - z_{\text{top}})$ denotes the fractional cloud height with $z' = 0$ for the cloud top and $z' = 1$ for the cloud base. Thus, the linear r_e profile is parameterized by r_{e1} at $z' = 0$ and r_{e2} at $z' = 1$ representing the cloud-top and cloud-base r_e, respectively. For retrievals of r_{e1} and r_{e2}, an optimal solution set is
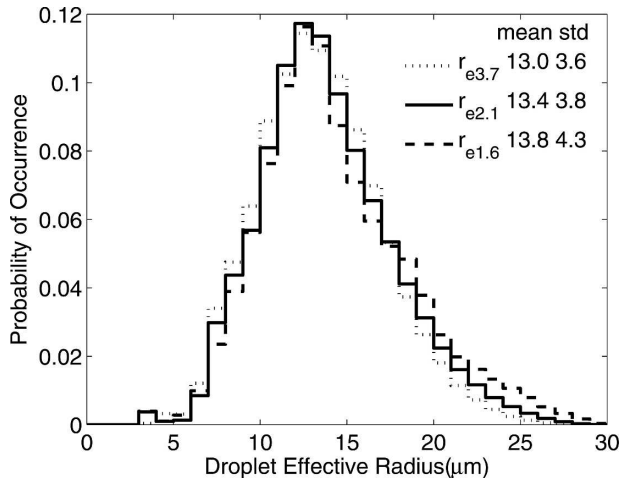
determined by matching the MODIS measurements with radiative transfer calculations at all three NIR channels, that is, 3.7, 2.1, and 1.6 μm. In their theoretical study, Chang and Li (2002) have analyzed the potential biases associated with the assumption of a linear r_e profile and reflectance error. They showed that the linear DER retrieval works best for median-thick cloud optical depths $\sim$10–28 and the retrieval mean biases are on the order of 1 μm for cloud top and slightly larger for cloud base if the DER profile has a close-to-linear variation. However, if the DER variation is very nonlinear, large biases will occur, in particular for cloud-base DER. Also, when clouds have large optical depth ($>$28), the quality of DER profile estimation does not change much for cloud top, but gets much worse for cloud base because the signal from cloud base is weak for such thick clouds. In these cases, the retrieved r_{e2} probably represents the middle portion of a thick cloud and does not represent for the cloud base. Over all, the uncertainties in r_{e2} can be larger by 2–3 factors than the uncertainties in r_{e1}.

Figure 3 shows the frequency distributions of the retrieved r_{e1} and r_{e2} for the data shown in Fig. 2. While the mean and standard deviation of the r_{e1} distribution are similar to those of the $r_{e3.7}$ distribution shown in Fig. 2, the mean and standard deviation of the r_{e2} distribution are much larger than those of the $r_{e2.1}$, $r_{e1.6}$, and r_{e1} distributions. Because of droplet absorption, the DER retrieved from a single NIR channel like $r_{e3.7}$ is more sensitive to the layer near the cloud top, which can cause biases in LWP calculations if r_e varies vertically. For a cloud with a decreasing DER profile (DDP) with height, that is, a smaller r_e toward the cloud top, the calculated LWP would be underestimated. On the con-
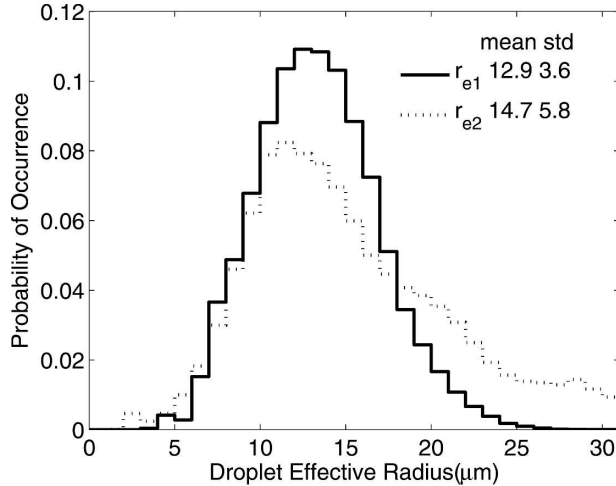
FIG. 3. Probability density function of the DER retrieved from a combination of three MODIS NIR channels.

TABLE 1. Statistics from the MODIS LWP estimations.

	$LWP_{3.7}$	$LWP_{2.1}$	$LWP_{1.6}$	LWPrep
Mean (mm)	0.115	0.117	0.120	0.124
Std (mm)	0.110	0.111	0.114	0.122
RMS with LWPrep (mm)	0.031	0.025	0.017	N/A

trary, for a cloud with an increasing DER profile (IDP), that is, a larger r_e toward the cloud top, the calculated LWP would be overestimated.

To show the effects of the different r_e on LWP estimations, different LWPs are calculated using $r_{e3.7}$, $r_{e2.1}$, and $r_{e1.6}$ with assumptions of a vertically constant r_e (hereafter referred to as $LWP_{3.7}$, $LWP_{2.1}$, and $LWP_{1.6}$) and using the linear r_e profile (hereafter referred to as LWPrep). Table 1 shows the comparisons of these LWPs. The RMS difference between LWPrep and $LWP_{3.7}$ is 0.031 mm, which is about 25% of the mean value. $LWP_{1.6}$ is the closest to LWPrep, but there is still an RMS difference of 0.017 mm. Therefore, the vertical variation of cloud DER has a considerable impact on the LWP estimation for the overcast warm cloud. As the above LWPs are derived from cloud optical depths and DER, the uncertainties in these LWP estimates are on the order of ~20%. Han et al. (1995) found a similar magnitude of uncertainties of 20% in their cloud LWPs derived using AVHRR cloud optical depths and DERs when they are compared with LWP estimation from an in situ microwave radiometer.

Note that 4 out of every 10 pixels in the along-track direction do not have correct radiance measurements at 1.6 μm for MODIS 1-km L1B data because of nonfunctional detectors at 1.6 μm. The average of measurements made by the nearest pixels is used here. This should not affect the results much because only overcast clouds are considered in this study, as explained in later sections.

b. AMSR-E retrieval

Cloud LWP has also been retrieved using satellite microwave remote sensing. In comparison with the vis-

ible/NIR retrievals, the microwave LWP estimation has a different physical basis, spatial resolution of field of view, and scanner viewing geometry. Several important algorithms, based on physical models, were developed for a variety of sensors, including the SSM/I (Lin and Rossow 1994; Weng and Grody 1994; Greenwald et al. 1995; Wentz 1997), the AMSU (Grody et al. 2001; Ferraro et al. 2005), and the AMSR-E (Ashcroft and Wentz 2000). Although a direct validation of such estimates has proven challenging (i.e., matching fine time/space upward-looking radiometer calculated LWP from small islands and ships with the large areal average LWP from the radiometer), most of these studies have concluded that the uncertainty of the passive microwave estimates are on the order of 0.02 mm under rain-free conditions. Further physical validation studies (Marchand et al. 2003; Ashcroft and Wentz 2000) indicate similar values. Wentz (1997) has analyzed the uncertainty of SSM/I LWP product. Atmospheric modeling error incurs uncertainty on order of 0.019 mm, radiometer noise incurs uncertainty on order of 0.007 mm, wind direction incurs uncertainty on order of 0.004 mm, and other sources incur uncertainty on order of 0.014 mm. The comparison with in situ measurements has shown that the total observed root-mean-square error of SSM/I LWP estimation is 0.025 mm.

Lin and Rossow (1994) compared the visible/NIR LWP derived from the International Satellite Cloud Climatology Project (ISCCP) cloud product with the SSM/I microwave LWP estimation. They found that the ISCCP LWP estimation is often larger than the SSM/I LWP estimation for tropical nonprecipitating clouds, but the difference is generally less than 10%. Greenwald and Christopher (2003) compared the LWP products derived from the Tropical Rainfall Measuring Mission (TRMM) Visible and Infrared Scanner (VIRS) with those derived from the TRMM Microwave Imager (TMI). They showed a clear-sky background bias in the TMI LWP estimation. After removal of the TMI background bias, a good agreement was found between the monthly mean LWPs from the two instruments. Ferraro et al. (2005) found that the LWP estimates from AMSU on NOAA satellites were somewhat smaller than ground-based in situ retrievals, which may be due to the extremely large AMSU footprint (~50 km).

The AMSR-E microwave measurements have 12 channels and 6 frequencies ranging from 6.9 to 89.0 GHz. Horizontally and vertically polarized radiation is measured separately at each frequency. The AMSR-E ocean product (version 4) from Wentz's algorithm is utilized in this study. The AMSR-E standard ocean algorithm (Ashcroft and Wentz 2000; Wentz 1997) retrieves sea surface temperature, surface wind speed, column water vapor, and LWP from the signals emitted by surface and atmospheric components at 6.9, 10.7, 18.7, and 36.5 GHz. The algorithm can retrieve LWP when there is no rainfall or if the rain rate is less than 2 mm h^{-1}. Although no direct validation results of the AMSR-E algorithm have been published in the open literature, the performance is generally accepted to be as good, if not better, than those documented by Wentz (1997) since it utilizes the same physical model and retrieval algorithm. However, the AMSR-E spatial resolution is better than SSM/I; thus the AMSR-E uncertainty may be slightly less that 0.025 mm.

The AMSR-E LWP product is compared with the LWPs derived from coincident MODIS measurements. Because of the highly variable emission of land surfaces, LWP estimations from passive satellite microwave observations are only applicable over oceans. The AMSR-E ocean product also provides rain flags, which are used to determine whether a cloud is raining or not. The rain flag is defined by an LWP threshold of 0.18 mm. This threshold is based on the comparison of SSM/I LWP retrievals with in situ rain observations (Wentz 1990; Wentz and Spencer 1998).

3. Results

In this study, the MODIS LWP estimates are compared with AMSR-E LWP estimates (LWP$_{MW}$). The AMSR-E and MODIS are on the *Aqua* satellite platform. MODIS has a cross-track scan while AMSR-E has a conical scan with a 53° viewing angle (Kawanishi et al. 2003). Temporal gaps of a few minutes exist between the two retrievals and the sensor viewing geometry is different for the two instruments. AMSR-E has a field of view (FOV) of approximately 13 km × 7 km at 37 GHz and the MODIS cloud product has a spatial resolution of 1 km at nadir. The MODIS measurements are matched to the larger AMSR-E footprint according to the navigation data. The statistical relationships between the MODIS and AMSR-E measurements are discussed to show the effect of the DER vertical variation on the MODIS LWP estimation and its potential for rain detection.

Since this study is primarily concerned with the impact of the vertical variation of DER on the estimation
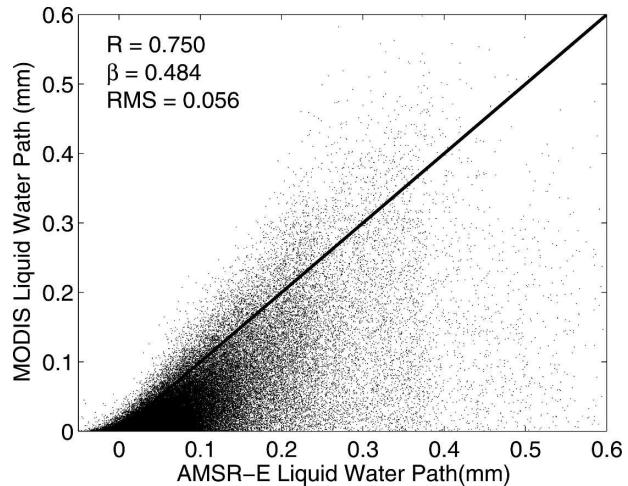

FIG. 4. Comparison between AMSR-E LWP and MODIS LWP$_{2.1}$ for all clouds. Here R is the correlation coefficient and β is the linear regression coefficient.

of MODIS LWP, the AMSR-E–derived LWP$_{MW}$ is used as a reference. However, there are many factors that may contribute to the differences between the two LWP estimations (Lin and Rossow 1994). The comparisons are first illustrated by comparing the MODIS LWP$_{2.1}$ with the AMSR-E LWP$_{MW}$. Figure 4 shows the comparisons between MODIS LWP$_{2.1}$ and AMSR-E LWP$_{MW}$ on the basis of the AMSR-E footprint. The correlation coefficient is 0.75 and the mean AMSR-E LWP$_{MW}$ is about 2 times larger than the MODIS LWP$_{2.1}$. The LWP comparisons from microwave and visible/NIR measurements can be significantly affected by the variability in cloud fraction, cloud optical depth, and cloud DER. These effects are demonstrated in the following subsections.

a. Effect of broken clouds

For each matched AMSR-E footprint, cloud fraction is determined based on the 1-km MODIS cloud mask by calculating the ratio of cloudy pixel number to total pixel number within the footprint. Figure 5 shows the impact of cloud fraction on the comparison between AMSR-E LWP$_{MW}$ and MODIS LWP$_{2.1}$. In the figure, the correlation coefficients, R, and associated slopes, β, from linear regression are derived and plotted against the different partitioning of AMSR-E cloud fraction. It is seen that cloud fraction has a large impact on the correlation between AMSR-E LWP$_{MW}$ and MODIS LWP$_{2.1}$. The two LWPs correlate well when the cloud fraction of AMSR-E footprint approaches 100%, but poorly when the cloud fraction is small.

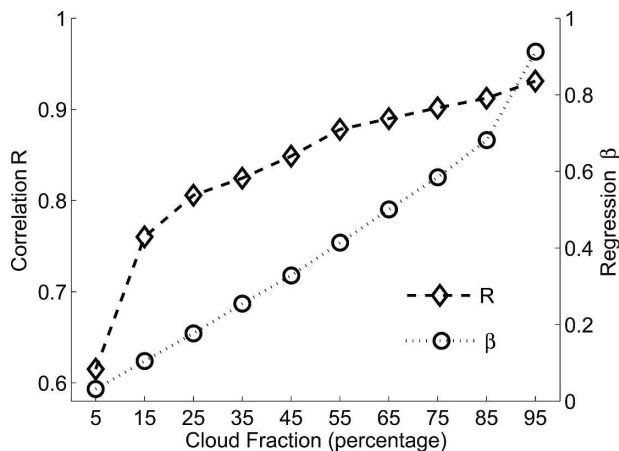It is a complex problem when broken clouds occur

FIG. 5. Effect of cloud fraction on the comparison between AMSR-E LWP and MODIS LWP$_{2.1}$. Here R is the correlation coefficient and β is the linear regression coefficient.
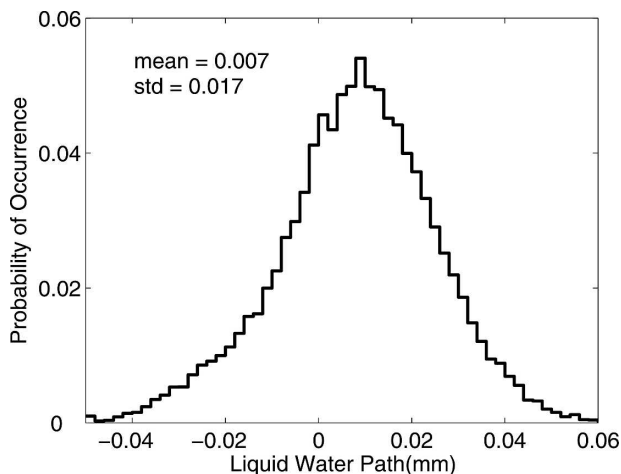

FIG. 6. Probability density function of AMSR-E LWP estimation for clear-sky conditions.

because the microwave LWP estimation may be significantly affected by the column water vapor amount, sea surface temperature, and surface wind speed. There is a background bias in microwave LWP estimations under clear-sky conditions (Lin and Rossow 1994; Greenwald and Christopher 2003). The background bias affects the accuracy of the AMSR-E LWP estimations for thin or broken clouds because the microwave signal from the cloud LWP is weak. To illustrate the clear-sky bias, Fig. 6 shows the frequency of occurrence of the AMSR-E LWP estimates when the MODIS indicates clear-sky conditions. As shown in the figure, the mean background bias is about 0.007 mm and the standard deviation of the bias is 0.017 mm for the single day's worth of data obtained between 40°N and 40°S over oceans.

After removing all nonuniform broken clouds (AMSR-E footprint cloud fraction < 100%), the agreement between AMSR-E and MODIS overcast LWP retrievals improves substantially with a correlation coefficient $R \sim 0.90$ and $\beta \sim 1.01$. Note that in the following sections (3b–3d), we focus on overcast clouds (AMSR-E footprint cloud fraction = 100%), for which the potential of using the DER vertical variation for warm rain detection and the effects on the cloud LWP estimation due to variability in cloud optical depth and DER are further examined.

b. Effect of cloud optical depth

Since cloud LWP depends strongly on cloud optical depth, variability of cloud optical depth within the AMSR-E footprint also affects the outcome of the comparison between the AMSR-E and MODIS LWPs. The microwave signal from optically thin clouds can be affected by the clear-sky background bias. The bias is due to uncertainties in column water vapor and surface emission that dominate the microwave measurements. In analyzing all overcast AMSR-E footprints, the data are divided into four groups based on the ISCCP cloud-type classification: $\tau < 3.6$, $\tau = 3.6$–9.4, $\tau = 9.4$–23, and $\tau > 23$. Table 2 shows the comparison of LWP$_{2.1}$ with LWP$_{MW}$ for clouds with various optical depths. The LWPs derived from the two instruments show poor agreement for clouds with optical depths less than 3.6. The comparisons show better agreement with increasing cloud optical depth. Optically thick clouds ($\tau > 23$) are excluded in the following studies because MODIS retrievals of DER at cloud base have large uncertainties for these clouds (Chang and Li 2002).

c. Effect of cloud DER vertical variation

Because of the effects of broken cloud and optical depth, overcast clouds with optical depths ranging between 3.6 and 23 are selected to investigate the impact of the DER vertical variation on LWP estimations and warm rain detection. The overcast cloud samples are mostly obtained in the eastern Pacific Ocean covered by extensive single-layer low-level clouds. Figure 7 is a scatterplot of MODIS LWP$_{2.1}$ as a function of AMSR-E LWP$_{MW}$, which includes all overcast AMSR-E footprints and cloud optical depths ranging

TABLE 2. Comparison of LWP$_{2.1}$ with LWP$_{MW}$ for clouds with various optical depths.

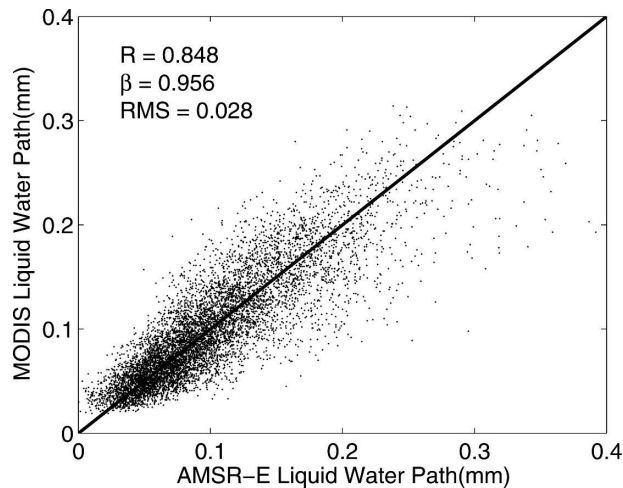|	$\tau < 3.6$	$3.6 \leq \tau < 9.4$	$9.4 \leq \tau < 23$	$\tau \geq 23$
R	0.517	0.709	0.762	0.687
β	0.621	0.856	0.979	1.111
RMS (mm)	0.018	0.021	0.035	0.072

FIG. 7. Comparison between AMSR-E LWP and MODIS LWP$_{2.1}$ for overcast clouds with cloud optical depth between 3.6 and 23. Here R is the correlation coefficient and β is the linear regression coefficient.

between 3.6 and 23. Table 3 shows the comparisons of LWP$_{MW}$ with LWP$_{3.7}$, LWP$_{2.1}$, LWP$_{1.6}$, and LWPrep. The different values of LWP$_{3.7}$, LWP$_{2.1}$, and LWP$_{1.6}$ show the effects of different retrievals of DER at the three NIR channels. As previously stated, the DER retrieved from a single NIR channel is biased toward the cloud top. Using a vertically constant DER, the LWP is overestimated for clouds with an IDP, and is underestimated for clouds with a DDP. Because the microwave LWP estimation measures the entire cloud layer, it is utilized to evaluate whether the DER profile improves the LWP estimation or not. From Table 3, LWPrep is better correlated with LWP$_{MW}$ than with LWP$_{3.7}$, LWP$_{2.1}$, and LWP$_{1.6}$. The regression coefficients do not change much because the vertical variation of DER has an opposite impact on LWP estimates for IDP clouds and DDP clouds. To show this effect in detail, clouds over AMSR-E footprints are separated into three categories: clouds with a neutral DER profile (NDP), and IDP clouds and DDP clouds based on $re1$ and $re2$. For DDP clouds $re2$ is 10% larger than $re1$, and it is 10% less than $re1$ for IDP clouds. For neutral clouds, the vertical variation of DER is within 10%.

TABLE 3. Comparison parameters of LWP$_{MW}$ with LWP$_{3.7}$, LWP$_{2.1}$, and LWP$_{1.6}$ for overcast warm clouds with optical depths ranging between 3.4 and 23.

	LWP$_{3.7}$	LWP$_{2.1}$	LWP$_{1.6}$	LWPrep
R	0.837	0.848	0.854	0.859
β	0.945	0.956	0.988	1.012
RMS (mm)	0.030	0.028	0.028	0.027

TABLE 4. Comparison between MODIS LWP and AMSR-E LWP for IDP, DDP, and NDP clouds.

		LWP$_{3.7}$	LWP$_{2.1}$	LWP$_{1.6}$	LWPrep
NDP	R	0.827	0.829	0.827	0.829
	β	1.026	1.017	1.030	1.029
	RMS	0.026	0.026	0.026	0.026
IDP	R	0.817	0.818	0.816	0.820
	β	1.126	1.092	1.086	1.052
	RMS	0.032	0.028	0.028	0.026
DDP	R	0.858	0.863	0.867	0.870
	β	0.888	0.914	0.959	1.001
	RMS	0.030	0.029	0.028	0.028

Table 4 shows the comparison between MODIS LWP and AMSR-E LWP for IDP, DDP, and NDP clouds. Because the vertical variation of DER causes the largest bias in LWP$_{3.7}$, LWP$_{3.7}$ is used to illustrate how the DER profile improves LWP estimations. LWP$_{2.1}$ and LWP$_{1.6}$ show similar biases of smaller magnitude.

LWP$_{3.7}$ is 12.6% larger than LWP$_{MW}$ for IDP clouds, 2.6% larger than LWP$_{MW}$ for NDP clouds, and 11.2% less than LWP$_{MW}$ for DDP clouds. Since the DER profile is the only criterion separating the data, it must be the primary cause for the differences. LWPrep, LWP$_{3.7}$, LWP$_{2.1}$, and LWP$_{1.6}$ are almost identical for NDP clouds because there are no vertical variations in the DER. The approximate 2.6% difference between MODIS LWP estimations and AMSR-E LWP estimations for NDP clouds is due to other uncertainty factors. So over the AMSR-E footprint, the bias caused by the vertical variation of DER in visible/NIR LWP estimations is about +10% (12.6%–2.6%) for IDP clouds and −13.8% (−11.2%–2.6%) for DDP clouds. LWPrep is 5.2% larger than LWP$_{MW}$ for IDP clouds and 0.1% larger than LWP$_{MW}$ for DDP clouds. Both differences are close to the 3% difference for NDP clouds. This means that the DER profile improves the LWP estimations and corrects the bias caused by the vertical variation of the DER. As previously stated, the uncertainties of LWP estimations are on the order of 0.025 mm or 20% for microwave methods and solar methods. The improvements made by DER profile are on a less magnitude as compared with uncertainties of the LWP estimation. Nevertheless, the improvements are systematic and physically sound, rather than a random noise. A magnitude of ±10% improvements in LWP estimation can be of significance in cloud water and radiation budget studies.

d. Implication for warm rain clouds

IR rain detection algorithms (Adler and Negri 1988; Arkin 1979) generally miss the presence of precipita-

tion in warm clouds because these algorithms depend on the cloud-top temperature. Microwave techniques cannot detect warm rain over land since the techniques rely on ice scattering over land (McCollum and Ferraro 2003). Over oceans, warm rain can be estimated from satellite microwave brightness temperatures because the surface emission is low and less variable (Wilheit et al. 2003). Recently, Ba and Gruber (2001) utilized the DER retrieved from the 3.9-μm channels on GOES satellites to detect warm rain clouds. As previously discussed, the DER retrieved from a single NIR channel is more sensitive to cloud-top than cloud-base values. In Fig. 3, the DER at the cloud base shows a wider spectrum than the DER at the cloud top, which may be explained by the cloud development phase: growing or decaying. Cloud droplet size increases with height during the developing stage due to condensation growth. Once a collision process starts, larger droplets tend to fall to the lower levels of the cloud. Therefore, the DER at cloud base is small for developing clouds and large for drizzling clouds. So the DER at the cloud base is more correlated with rainfall than DER at the cloud top. There were some previous studies that utilized the vertical DER variation to differentiate precipitating/nonprecipitating clouds (Shao and Liu 2004; Matsui et al. 2004). These studies combined microwave observation and shortwave observation to infer the vertical variation of DER. Chang and Li's algorithm captures the trend of the vertical DER variation from observations of multi-NIR channels. A preliminary investigation was done using the rain flag defined in the AMSR-E ocean product to show the potential of the linear DER profile retrieval for warm rain detection.

Figure 8 shows the distribution of DER at cloud base and cloud top for raining and nonraining clouds, respectively, which are defined by the AMSR-E rain flag. Raining causes a DER increase of 3.5 μm at the cloud top (Fig. 8a) and a DER increase of 7 μm at the cloud base (Fig. 8b). So DER at cloud base is more effective for rain detection. For example, if we define a threshold of 14 μm for raining clouds (Rosenfeld and Gutman 1994), the DER at the cloud base correctly classifies 87.0% of AMSR-E–detected rains, while the DER at the cloud top classifies only 64.4% of AMSR-E–detected rains. For some AMSR-E–detected raining clouds, the DER at the cloud base can be as small as 10 μm. These clouds could be partially raining, while overall small DER is evident because of the effect of the nonraining part of the clouds. However, based on the same 14-μm raining threshold, the false raining detection rate is 22.7% using the DER at the cloud top and 30.6% using the cloud-bottom DER. If the DER threshold is increased to 20 μm, the false detection rate
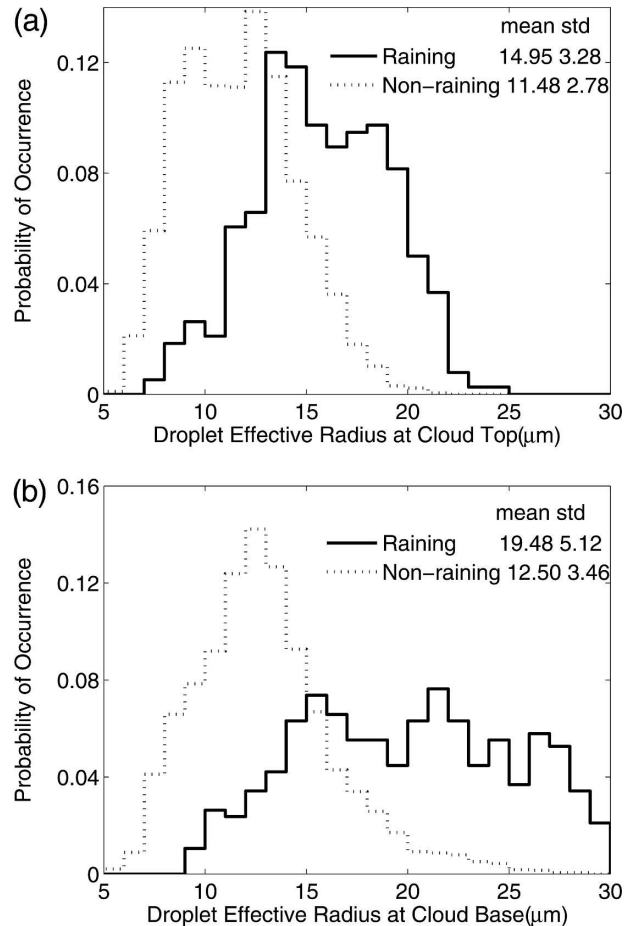

FIG. 8. Probability density function of DER at cloud tops and cloud bases for raining and nonraining clouds over AMSR-E footprints.

is considerably reduced, at the expense of missing some raining clouds. The false detection may be due to the AMSR-E sensitivity problem. Many of these AMSR-E–defined nonraining clouds could have very light rain or drizzle that evaporates before reaching the ground. Figure 9 shows the distribution of the DER differences between the cloud top and the cloud base. Raining clouds generally have larger DER at the cloud base than at the cloud top. This result is consistent with in situ observation (Martin et al. 1994). Use of -2 μm in the DER difference appears effective in separating the majority of raining and nonraining clouds, although there are some uncertainties. The uncertainties could be caused by partially raining clouds, as well as AMSR-E sensitivity problems. Development of a rain detection algorithm is beyond the scope of this study.

4. Concluding remarks

Traditionally, satellite retrievals of DER are based on satellite reflectance measurements from a single
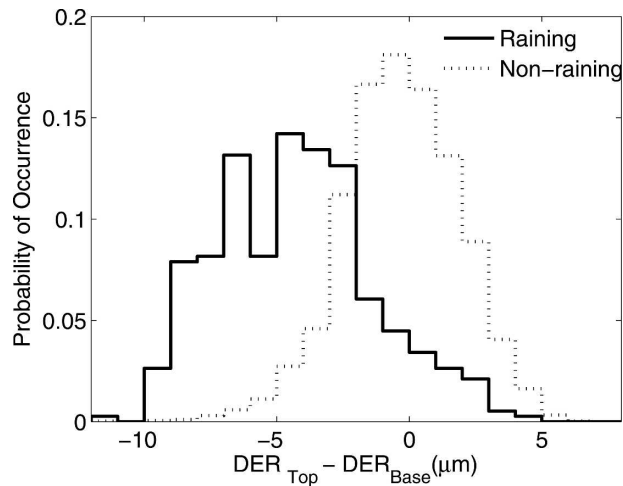
FIG. 9. Probability density function of DER differences between cloud top and cloud base for raining and nonraining clouds over AMSR-E footprints.

NIR channel, plus visible and thermal infrared data. They cannot describe the vertical variation of DER from the cloud top to the cloud base. When computing cloud LWP from cloud optical depth and DER, the latter is effectively assumed to be a constant. By analyzing a single day's worth of MODIS and AMSR-E products over the tropical ocean for warm and overcast clouds with optical depths ranging between 3.6 and 23, this investigation demonstrates that assuming a constant cloud DER can incur biases in the calculations of LWP. It is also shown that accounting for the vertical variation of DER profiles can reduce the mean biases, though the DER vertical variation is not the only source of uncertainties in cloud LWP estimation. These findings are based on comparisons between LWP retrieved from the AMSR-E microwave measurements and LWP computed from the MODIS visible/NIR cloud optical depth and DER retrievals. AMSR-E LWP products are utilized for comparisons because microwave radiometer observes the whole cloud column. However, uncertainties in microwave retrievals like the AMSR-E can also be incurred from error sources like ocean surface emissions, cloud properties, radiometric calibrations, and beam filling problems. Also the data sample utilized in this investigation is very limited. Further study is required when more accurate LWP products become available in the future.

Despite the fact that the result shows that improvements on the MODIS LWP calculations with DER vertical variation are only on the order of 10% for the utilized data samples, the improvements are systematic and physically sound. The DER profile algorithm could be applied to the future GOES-R satellite. The re-

trieved DER vertical variations from multiple NIR channels can help in detecting rain, especially warm rain over land, which is problematic for existing passive microwave techniques. This is very important for global and regional hydrological research because of the predominance of rainfalls occurring from warm cloud tops in some climate regimes. The relationship between the DER profile and the raining process can also help with research concerning the aerosol indirect effect. All previous investigations utilized the DER retrieved from a single NIR channel to study the effect of aerosols on cloud DER and raining. However, the DER retrieved from a single channel is biased toward the cloud top. Aerosols generally have more effect on the cloud base. The DER at the cloud base and the DER profile are proved to be more related to the raining process than the DER at the cloud top.

REFERENCES

Adler, R. F., and A. J. Negri, 1988: A satellite infrared technique to estimate tropical convective and stratiform rainfall. *J. Appl. Meteor.,* **27,** 30–51.

Arkin, P. A., 1979: The relationship between fractional coverage of high cloud and rainfall accumulations during GATE over the B-scale array. *Mon. Wea. Rev.,* **107,** 1382–1387.

Ashcroft, P., and F. J. Wentz, 2000: AMSR algorithm theoretical basis document. RSS Tech. Rep. 121599B-1, 27 pp.

Ba, M., and A. Gruber, 2001: GOES Multispectral Rainfall Algorithm (GMSRA). *J. Appl. Meteor.,* **40,** 1500–1514.

Chang, F.-L., and Z. Li, 2002: Estimating the vertical variation of cloud droplet effective radius using multispectral near-infrared satellite measurements. *J. Geophys. Res.,* **107,** 4257, doi:10.1029/2001JD000766.

——, and ——, 2003: Retrieving vertical profiles of water-cloud droplet effective radius: Algorithm modification and preliminary application. *J. Geophys. Res.,* **108,** 4763, doi:10.1029/2003JD003906.

——, ——, and S. A. Ackerman, 2000: Examining the relationship between cloud and radiation quantities derived from satellite observations and model calculations. *J. Climate,* **13,** 3842–3859.

Derber, J. C., D. F. Parrish, and S. J. Lord, 1991: The new global operational analysis system at the National Meteorological Center. *Wea. Forecasting,* **6,** 538–547.

Ferraro, R. R., and Coauthors, 2005: NOAA operational hydrological products derived from the AMSU. *IEEE Trans. Geosci. Remote Sens.,* **43,** 1036–1049.

Greenwald, T. J., and S. A. Christopher, 2003: Methods for evaluating microwave-derived satellite liquid water products. Pre-

prints, *12th Conf. on Satellite Meteorology and Oceanography,* Long Beach, CA, Amer. Meteor. Soc., CD-ROM, P4.3.

——, G. L. Stephens, S. A. Christopher, H. Vonder, and H. Thomas, 1995: Observations of the global characteristics and regional radiative effects of marine cloud liquid water. *J. Climate,* **8,** 2928–2946.

Grody, N. C., J. Zhao, R. Ferraro, F. Weng, and R. Boers, 2001: Determination of precipitable water and cloud liquid water over oceans from the NOAA-15 advanced microwave sounding unit. *J. Geophys. Res.,* **106,** 2943–2954.

Han, Q., W. B. Rossow, and A. A. Lacis, 1994: Near-global survey of effective droplet radii in liquid water clouds using ISCCP data. *J. Climate,* **7,** 465–497.

——, ——, R. Welch, A. White, and J. Chou, 1995: Validation of satellite retrievals of cloud microphysics and liquid water path using observation from FIRE. *J. Atmos. Sci.,* **52,** 4183–4195.

——, ——, J. Chou, and R. M. Welch, 1998: Global survey of the relationships of cloud albedo and liquid water path with droplet size using ISCCP. *J. Climate,* **11,** 1516–1528.

Hansen, J. E., and L. D. Travis, 1974: Light scattering in planetary atmospheres. *Space Sci. Rev.,* **16,** 527–610.

Harrison, E. F., P. Minnis, B. R. Barkstrom, V. Ramanathan, R. D. Cess, and G. G. Gibson, 1990: Seasonal variation of cloud radiative forcing derived from the earth radiation budget experiment. *J. Geophys. Res.,* **95,** 18 687–18 703.

Hartmann, D. L., M. E. Ockert-Bell, and M. L. Michelsen, 1992: The effect of cloud type on the Earth's energy balance: Global analysis. *J. Climate,* **5,** 1281–1304.

Kaufman, Y. J., and T. Nakajima, 1993: Effect of Amazon smoke on cloud microphysics and albedo-analysis from satellite imagery. *J. Appl. Meteor.,* **32,** 729–743.

Kawanishi, T., and Coauthors, 2003: The Advanced Microwave Scanning Radiometer for the Earth Observing System (AMSR-E), NASDA's contribution to the EOS for global energy and water cycle studies. *IEEE Trans. Geosci. Remote Sens.,* **41,** 184–193.

King, M. D., S.-C. Tsay, S. E. Platnick, M. Wang, and K.-N. Liou, cited 1997: Cloud retrieval algorithms for MODIS: Optical thickness, effective particle radius, and thermodynamic phase. MODIS Algorithm Theoretical Basis Doc. ATBD-MOD-05, 83 pp. [Available online at http://modis.gsfc.nasa.gov/data/atbd/atbd_mod05.pdf.]

——, and Coauthors, 2003: Cloud and aerosol properties, precipitable water, and profiles of temperature and humidity from MODIS. *IEEE Trans. Geosci. Remote Sens.,* **41,** 442–458.

Lin, B., and W. B. Rossow, 1994: Observations of cloud liquid water path over oceans: Optical and microwave remote sensing methods. *J. Geophys. Res.,* **99,** 20 907–20 927.

Marchand, R., T. Ackerman, E. R. Westwater, S. A. Clough, K. Cady-Pereira, and J. C. Liljegren, 2003: An assessment of microwave absorption models and retrievals of cloud liquid water using clear-sky data. *J. Geophys. Res.,* **108,** 4773, doi:10.1029/2003JD003843.

Martin, G. M., D. W. Johnson, and A. Spice, 1994: The measurement and parameterization of effective radius of droplets in warm stratocumulus clouds. *J. Atmos. Sci.,* **51,** 1823–1842.

Matsui, T., H. Masunaga, R. A. Pielke Sr., and W.-K. Tao, 2004: Impact of aerosols and atmospheric thermodynamics on cloud properties within the climate system. *Geophys. Res. Lett.,* **31,** L06109, doi:10.1029/2003GL019287.

McCollum, J. R., and R. R. Ferraro, 2003: Next generation of NOAA/NESDIS SSM/I, TMI, and AMSR-E microwave land rainfall algorithms. *J. Geophys. Res.,* **108,** 8382, doi:10.1029/2001JD001512.

Menzel, W. P., and L. E. Gumley, cited 1998: MODIS atmospheric profile retrieval. Algorithm Theoretical Basis Doc., 38 pp. [Available online at http://krsc.kari.re.kr/sub/satellite/download/satellite_04/MODIS/atbd_mod07.pdf.]

Miles, N. L., J. Verlinde, and E. E. Clothiaux, 2000: Cloud droplet size distributions in low-level stratiform clouds. *J. Atmos. Sci.,* **57,** 295–311.

Nakajima, T., and M. D. King, 1990: Determination of the optical thickness and effective particle radius of clouds from the reflected solar radiation measurements. Part I: Theory. *J. Atmos. Sci.,* **47,** 1878–1893.

Platnick, S., 2000: Vertical photon transport in cloud remote sensing problems. *J. Geophys. Res.,* **105,** 22 919–22 935.

——, and F. P. J. Valero, 1995: A validation study of a satellite cloud retrieval during ASTEX. *J. Atmos. Sci.,* **52,** 2985–3001.

Rosenfeld, D., and G. Gutman, 1994: Retrieving microphysical properties near the tops of potential rain clouds by multispectral analysis of AVHRR data. *Atmos. Res.,* **34,** 259–283.

Rossow, W. B., 1989: Measuring cloud properties from space: A review. *J. Climate,* **2,** 201–213.

——, L. C. Garder, and A. A. Lacis, 1989: Global, seasonal cloud variations from satellite radiance measurements. Part I: Sensitivity of analysis. *J. Climate,* **2,** 419–458.

Shao, H., and G. Liu, 2004: Detecting drizzle in marine warm clouds using combined visible, infrared, and microwave satellite data. *J. Geophys. Res.,* **109,** D07205, doi:10.1029/2003JD004286.

Stephens, G. L., 1999: Radiative effects of clouds and water vapor. *Global Energy and Water Cycle,* K. A. Browning and R. J. Gurney, Eds., Cambridge University Press, 71–90.

Weng, F., and N. G. Grody, 1994: Retrieval of cloud liquid water using the special sensor microwave imager (SSM/I). *J. Geophys. Res.,* **99,** 25 535–25 551.

Wentz, F. J., 1990: SBIR phase II report: West coast storm forecasting with SSM/I. RSS Tech. Rep. 033190, 378 pp.

——, 1997: A well-calibrated ocean algorithm for SSM/I. *J. Geophys. Res.,* **102,** 8703–8718.

——, and R. W. Spencer, 1998: SSM/I rain retrievals within a unified all-weather ocean algorithm. *J. Atmos. Sci.,* **55,** 1613–1627.

Wilheit, T., C. Kummerow, and R. Ferraro, 2003: Rainfall algorithms for AMSR-E. *IEEE Trans. Geosci. Remote Sens.,* **41,** 204–214.